Oceanic Response to Changes in the Latitude of the Southern Hemisphere Subpolar Westerly Winds

PETER R. OKE* AND MATTHEW H. ENGLAND

Centre for Environmental Modelling and Prediction, School of Mathematics, University of New South Wales, Sydney, Australia

(Manuscript received 12 February 2003, in final form 21 August 2003)

ABSTRACT

The oceanic response to imposed changes in the latitude of the subpolar westerly winds (SWWs) over the Southern Ocean is assessed in a global ocean model. The latitude changes are achieved by applying a zonally uniform zonal wind stress anomaly that is quasi-sinusoidal in latitude, with a positive (negative) band to the south (north) of about 50°S. This form of anomaly is chosen because it projects onto the Antarctic Oscillation, also known as the Southern Hemisphere annular mode, that is known to have a long-term trend. The response to both long-term trend and quasi-decadal periodic changes is examined in the latitude of the SWWs. In the long-term trend case, a 5.4° poleward shift of the SWWs over a 100-yr simulation is found to cause the poleward heat transport to increase by an average of 25% between 50°S and the equator. This change is primarily due to greater northward Ekman transport of cold water and its associated cooling of Subantarctic Mode Water (SAMW) by up to 0.5°C in the central-south Pacific. The authors also find that the rate of formation of Antarctic Intermediate Water increases as the SWWs shift poleward, resulting in cooling and freshening at intermediate depths. In the periodic experiment, where the SWWs axis has a range of 5.4° latitude, the poleward heat transport, North Atlantic Deep Water outflow and the overturning of Antarctic Bottom Water are all modulated by 20%–30%. Significant cooling is found at intermediate and upper-level water depths in the trend experiment and temperature fluctuations with a range of up to 0.4°C in the periodic experiment. These changes are of the same magnitude and form as that recently observed at intermediate depths in the Southern Ocean. The authors conclude that latitudinal shifts of the SWWs may play a significant role in generating observed temperature fluctuations at intermediate water depths.

1. Introduction

A recent report of temperature trends at intermediate water depths in the Southern Ocean noted higher than expected warming at high latitudes and cooling in several regions at midlatitudes (Gille 2002). Thresher et al. (2003, manuscript submitted to *Geophys. Res. Lett.*, hereafter T03) also observed cooling off Tasmania, in addition to quasi-decadal, or longer, temperature fluctuations. Both Gille (2002) and T03 hypothesize that aspects of their observations may be explained by variations in the wind stress field over the Southern Ocean. In support of this, climate records off southern Australia show that the zonal wind bands and subtropical ridge have shifted poleward by about 5° latitude over the last century (Das 1956; Thresher 2002). Indeed, climate change predictions suggest that this trend is likely to continue under enhanced greenhouse gas conditions (e.g., Whetton et al. 1996; Fyfe et al. 1999; Kushner et al. 2001; Cai et al. 2003). Additionally, there is some evidence of quasi-decadal variations in the strength of the zonal winds at several sites at high Southern Hemisphere latitudes that could be explained by cyclical latitudinal shifts in the Southern Hemisphere zonal wind bands (Harris et al. 1988; Thresher 2002). The goal of this study is to investigate the impacts of changes in the wind field over the subpolar Southern Hemisphere on ocean circulation and water mass properties.

The particular focus of our study is the oceanic response to changes in the latitude of the Southern Hemisphere subpolar westerly winds (SWWs). This is achieved by applying a zonally uniform zonal wind stress anomaly that projects onto the Antarctic Oscillation (AAO), also known as the Southern Hemisphere annular mode. The AAO refers to coherent oscillations of sea level pressure (SLP) in the Southern Hemisphere that result from internal atmospheric dynamics, where the eddy–mean flow interactions result in fluctuations in the SWWs on synoptic time scales (e.g., Hartmann and Lo 1998; Limpasuvan and Hartmann 1999). There is evidence that suggests that ozone, greenhouse gas, and solar events induce changes that have a projection

* Current affiliation: CSIRO Marine Research, Hobart, Tasmania, Australia.

Corresponding author address: Dr. Peter R. Oke, CSIRO Marine Research, GPO Box 1538, Castray Esplanade, Hobart TAS 7001 Australia.
E-mail: peter.oke@csiro.au

onto the AAO pattern of SLP (e.g., Rogers and van Loon 1982; Hartmann et al. 2000). However, these changes are presumably separate and distinct both in mechanism and time scale from the AAO. Despite the observational evidence that the AAO has a long-term trend (Thompson et al. 2000), we shall refer to the synoptic time-scale wind variations as the AAO and all longer time-scale wind variations that project onto the AAO as those associated with the SWWs.

The ocean's response to the AAO has previously been investigated by Hall and Visbeck (2002) using a climate model. The approach utilized in their study was to identify correlations between the time series of the first-mode empirical orthogonal function of SLP, representing variations of the AAO, with different modeled oceanic variables and calculating regression coefficients in order to quantify these relationships. Hall and Visbeck provide many useful insights into the role of the AAO, for example, demonstrating that it influences the poleward heat transport and sea ice variability in the Southern Hemisphere and the rate of overturning in the Deacon cell on synoptic time scales. Watterson (2000) also used a climate model to identify the effects of the AAO on the Deacon cell overturning. However, by not explicitly imposing variations in the AAO winds, these analyses of climate model output are unable to isolate wind effects from other climate forcings. We think a good complementary approach to this problem involves a sensitivity study of the ocean's response to imposed changes in the latitude of the SWWs using an ocean-only model. While the use of an ocean-only model has the disadvantage of lacking realistic feedbacks between the ocean, ice, and atmosphere, it has the advantage of simplicity in that different aspects of the wind forcing can be systematically changed in order to isolate the effects of winds from other forcings (such an approach is commonly adopted; e.g., Toggweiler and Samuels 1993, 1995; McDermott 1996; Rahmstorf and England 1997; Ribbe 1999). To this end, we utilize a coarse-resolution model to investigate the ocean's response to various idealized changes in the latitude of the SWWs.

The SWWs have a strong influence in driving flow in the Antarctic Circumpolar Current (ACC; Stommel 1957; Gnanadesikan and Hallberg 2000), as well as controlling the overturning in the Deacon cell. Indirectly, the SWWs are thought to influence the rate of production and export of North Atlantic Deep Water (NADW; Toggweiler and Samuels 1995, 1993; McDermott 1996; Nof 2000), Antarctic Intermediate Water (AAIW; Ribbe 1999; Santoso and England 2003, manuscript submitted to *J. Phys. Oceanogr.*) and Antarctic Bottom Water (AABW; Rahmstorf and England 1997), as well as controlling *T*–*S* properties of Subantarctic Mode Water (SAMW; Rintoul and England 2002). In addition, the wind stress curl associated with the SWWs plays a key role in driving the Southern Hemisphere subtropical gyres in each ocean basin. Clearly, the SWWs play an important role in driving the global ocean circulation.

Several modeling studies have previously investigated the ocean's response to an imposed variation in the zonal wind stress over the Southern Ocean (e.g., Toggweiler and Samuels 1993, 1995; McDermott 1996; Rahmstorf and England 1997). However, none that we are aware of have addressed changes in the latitude of the SWWs. Such changes could occur during a low-frequency expansion or contraction of the AAO that might be induced by anthropogenic climate change (e.g., Fyfe et al. 1999) or natural quasi-decadal variability (e.g., van Loon and Labitzke 1998), possibly associated with the Antarctic Circumpolar Wave (White and Peterson 1996), or through teleconnections to the El Niño–Southern Oscillation (e.g., Smith and Stearns 1993; Carleton 2003). In this paper we present results from two anomaly experiments. The first experiment involves a gradual poleward shift in the SWWs, such as that observed by Das (1956), Thompson et al. (2000), Thresher (2002), and Thompson and Solomon (2002), and simulated by Whetton et al. (1996), Fyfe et al. (1999), Kushner et al. (2001), and Cai et al. (2003). A poleward shift of 5.4° is chosen to be consistent with the results referred to above. The second experiment involves time-varying periodic latitudinal shifts in the SWWs to examine the impact of quasi-decadal variations. This experiment is motivated by the analyses presented by Harris et al. (1998), who noted a clear cyclical pattern in the zonal winds off Hobart, Tasmania, between 1945 and 1985. Subsequently, Thresher (2002) demonstrated similar in-phase cycling of meridional pressure gradients over Australia, South America, and South Africa, hypothesizing that there is a quasi-decadal periodicity in the latitude of the SWWs. We have chosen to use a range of 5.4° in order to utilize the same spatial wind stress anomalies as the first experiment introduced above. It is also worth noting that Jones and Widmann (2003) reconstructed a time series of an AAO index (representing temporal variations in the strength and position of the SWWs associated with the AAO) from instrument and tree-ring measurements and found evidence of variability on decadal time scales (their Fig. 4).

The outline of the rest of this paper is as follows. A description of the model configuration and the numerical experiments is presented in section 2. Results are presented in section 3. In section 4 we discuss the model simulations further, with particular reference to the proposed mechanisms to explain the observed cooling at intermediate depths at midlatitudes in the Southern Ocean. Finally, our conclusions are summarized in section 5.

2. Model description

a. Model configuration

The ocean model used in this study is the Bryan–Cox ocean general circulation model (Bryan 1969; Cox

TABLE 1. Summary of experiments; TA refers to the trend anomaly experiment; PA refers to the periodic anomaly experiment. Both TA and PA are integrated from year 4300 of CNTRL.

Expt	Description	Run length (yr)
CNTRL	Control experiment	4400
TA	Trend toward a 5.4° poleward shift of the SWWs	100
PA	Idealized 11-yr periodic latitudinal shifts in the SWWs	100

1984; Pacanowski et al. 1995). The model geometry resolves the flow around the major continents and accommodates flow through the Indonesian Archipelago. The model domain consists of a near-global coverage of the World Ocean extending from the Antarctic continent to 80°N. The model topography represents a smoothed version of the real World Ocean bottom topography and is derived from the 1° atlas documented by Smith and Sandwell (1997). The model grid spacing is 1.8° latitude by 3.6° longitude with 21 unequally spaced vertical levels with vertical resolution that varies from 50 m near the surface to 385 m in the ocean's abyss.

The effects of mesoscale processes are taken into account implicitly by parameterizations of subgrid-scale mixing of momentum and tracers. The horizontal and vertical viscosity coefficients are taken to be constants independent of depth (2.0×10^9 cm^2 s^{-1} and 50 cm^2 s^{-1}, respectively). The vertical diffusivity is lowest in the surface layer (0.3 cm^2 s^{-1}) and increases below the thermocline (after Bryan and Lewis 1979) towards a maximum of 1.3 cm^2 s^{-1}. Because there is little physical justification for inclusion of horizontal diffusivity (e.g., McDougall and Church 1986) we utilize the scheme described by Gent and McWilliams (1990, hereafter GM) and Gent et al. (1995) for representing adiabatic transport effects of baroclinic eddies. A highly desirable feature of this scheme is that it allows the model to be run with zero horizontal diffusivity. Several studies have demonstrated quantitative improvements when this scheme is utilized, particularly in the Southern Ocean (e.g., Danabasoglu et al. 1994; England 1995; Danabasoglu and McWilliams 1995; Robitaille and Weaver 1995; Hirst and McDougall 1996; England and Hirst 1997). The isopycnal thickness diffusivity is 1.0×10^7 cm^2 s^{-1} (after Danabasoglu et al. 1994; Hirst and McDougall 1996). The along-isopycnal mixing tensor of Redi (1982) is also adopted to approximate the ocean's tendency to mix along surfaces of constant density. Convection is treated implicitly in the model in order to vertically mix temperature and salinity wherever density inversions occur.

The currents are initially at rest and potential temperature (T) and salinity (S) fields are spatially uniform with values of 4°C and 34.7 practical salinity units (psu). The ocean is forced at the sea surface by seasonally varying climatological boundary conditions of T, S, and wind stress. The wind stress in our control experiment is derived from the climatology of Hellerman and Rosenstein (1983). Surface T–S fields are damped towards the monthly climatology of Levitus (1982) with uniform restoring time scales of 30 and 50 days, respectively. The restoring salinity is increased to 35 psu for all ocean grid points south of 74°S during three wintertime months (similar to England 1993) in order to achieve more realistic deep- and bottom-water properties off Antarctica. The ocean model is integrated with a time step of 6 h for T and S and 15 min for velocity components and the free surface. The integration of the control experiment is run out to 4400 years in order to ensure that an equilibrated state has been reached.

b. Experimental design

Observations over the last century have shown that the zonal wind band associated with the SWWs has shifted poleward by approximately 5° since the early 1900s (Das 1956; Thresher 2002). Additionally, several climate change predictions suggest that the SWWs are likely to shift by 5° or more under enhanced greenhouse gas conditions (e.g., Whetton et al. 1996; Fyfe et al. 1999; Kushner et al. 2001; Cai et al. 2003), and there have been several reports of quasi-decadal oscillations in the SWWs (Harris et al. 1988; Thresher 2002; Jones and Widmann 2003). Motivated by these reports, we perform two experiments in addition to the control: (i) a *trend* anomaly experiment that involves a gradual poleward shift in the SWWs, representing the effects of anthropogenic climate change, and (ii) a *periodic* anomaly experiment that involves an oscillating latitudinal shift in the SWWs, representing natural quasi-decadal variability. A summary of these experiments is presented in Table 1. Each anomaly experiment is run for 100 years and is initialized from the equilibrated control solution at year 4300. The zonal wind field is the only aspect of the model configuration that is changed from the control to the anomaly experiments.

The zonally averaged zonal wind stress and wind stress curl at the end of the trend anomaly experiment is compared to the control in Fig. 1. The trend anomaly experiment (hereafter TA) involves the addition of an idealized zonal wind stress anomaly that is ramped up from zero over a 100-yr simulation. This anomaly is quasi-sinusoidal in latitude [similar to that diagnosed by Fyfe (2003) using a climate model], with a zero crossing near 50°S and the maximum positive (negative) anomaly of 0.04 Pa near 60°S (40°S). In this experiment the center of the SWWs gradually shifts polewards by 5.4° over the course of the simulation. Importantly, the strength of the annual-average maximum zonal wind

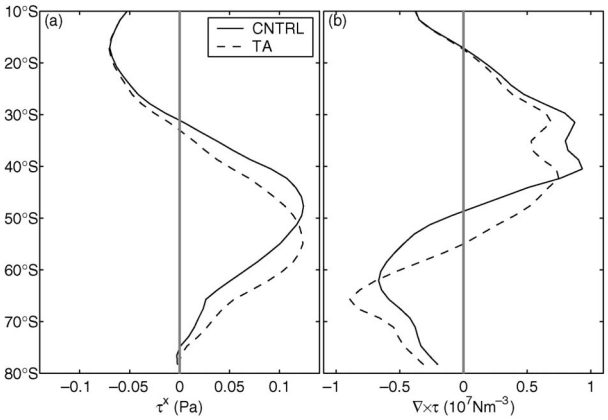

FIG. 1. The zonally averaged (a) zonal wind stress and (b) wind stress curl for CNTRL and at the end of TA. Fields for CNTRL (TA) are the same as during the northernmost (southernmost) excursions of the SWWs in experiment PA.

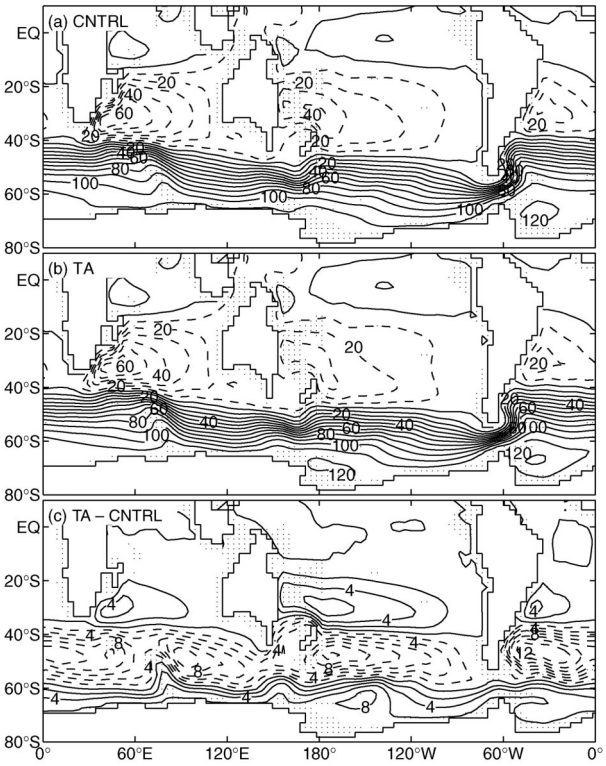

FIG. 2. The horizontal transport streamfunction for (a) CNTRL, (b) TA, and (c) the difference field, TA − CNTRL. Contour intervals are 10 Sv in (a) and (b), and 2 Sv in (c); positive is solid, negative is dashed, zero is bold; stippled areas denote regions shallower than 3000 m.

stress remains unchanged throughout the experiment. This is in contrast to the profile diagnosed by Fyfe (2003), who found that in addition to the poleward shift, the SWWs also strengthen under enhanced greenhouse gas conditions. The ocean's response to strengthened zonal winds is well documented (e.g., Toggweiler and Samuels 1995; Rahmstorf and England 1997).

The periodic anomaly experiment (hereafter PA) involves the application of the same zonal wind stress anomalies used in TA, only now the winds periodically shift toward and away from Antarctica with a period of 11 yr. Evidence of quasi-decadal cycling in the SWWs has been documented by Harris et al. (1998) and Thresher (2002).

In order to gain insight into the dominant mechanisms that cause the changes between the control (CNTRL) and the anomaly experiments, we have utilized a series of passive tracers. Specifically, we want to monitor changes in the rate of production of SAMW and AAIW caused by the shifts in the SWWs. To this end, we utilize two separate tracer fields initialized to zero at year 4300. Each passive tracer is restored to zero at all surface points except in the designated production regions where the tracer is restored to unity. We define two separate regions nominally covering the production locations for SAMW and AAIW. These are set to latitudinal bands at 40°–50°S and 50°–60°S, respectively. Hereafter, these tracers are referred to as tracer MW and IW, respectively. Each tracer is integrated in an identical fashion to *T*–*S* so that processes such as advection, vertical mixing, along-isopycnal, and GM transport as well as convection are all taken into account.

In addition to the experiments introduced, we have also examined the oceanic response to wind stress anomalies over synoptic time scales. Specifically, we applied high-frequency wind stress anomalies over the subpolar Southern Ocean that reflect synoptic-scale variability in the AAO and high-latitude storms. As above, these experiments were not run in a coupled model configuration. We found that, while some time-varying signature appears in the oceanic response to high-frequency wind anomalies, the long-term mean response is rather small. In particular, the temperature changes were restricted to the upper ocean where the annual mean temperature changes were at most 0.4°C at 100-m depth in the Southern Ocean. Overall we found that the mean response of the model ocean was rather insensitive to synoptic-scale variability in the wind forcing fields. This is probably due to the dissipative nature of our coarse-resolution model and the fact that our model is run in uncoupled mode. We suggest that an eddy permitting/resolving model with some simple coupled atmosphere would be a more appropriate tool for assessing the role of high-frequency wind variability over the Southern Ocean.

3. Results

a. The control experiment

All fields presented in this section are annual means. The horizontal transport streamfunction in the Southern Hemisphere is shown for CNTRL in Fig. 2a. The model simulates the major western boundary currents and throughflow transports (listed in Table 2) at rates com-

TABLE 2. Maximum transports in Sv of the major Southern Hemisphere western boundary currents and the Drake Passage and Indonesian throughflows in CNTRL and TA, and the range of transports in PA.

Current	Max transport (Sv)		Transport range (Sv)
	CNTRL	TA	PA
Brazil	30.1	26.0	4.7
East Australia	22.5	16.5	4.4
Agulhas	68.4	64.1	5.9
Drake Passage (ACC)	126.4	132.1	3.4
Indonesian Passage	19.1	18.6	1.4

parable to observed estimates. Specifically, reported estimates from observations for the Southern Hemisphere suggest that the typical range of transport in the Brazil Current is 30–56 Sv (Sv $\equiv 10^6$ m^3 s^{-1}) (Maamaatuaiahutapu et al. 1998); the East Australian Current is 17–27 Sv (Mata et al. 2000); the Agulhas Current is 40–100 Sv (Beal and Bryden 1999); the ACC through Drake Passage is 98–154 Sv (Whitworth et al. 1982; Whitworth 1983; Orsi et al. 1995); and the flow through the Indonesian Archipelago is 2–18 Sv (Fieux et al. 1996). In each case, the modeled transports in CNTRL are within, or close to, the expected range.

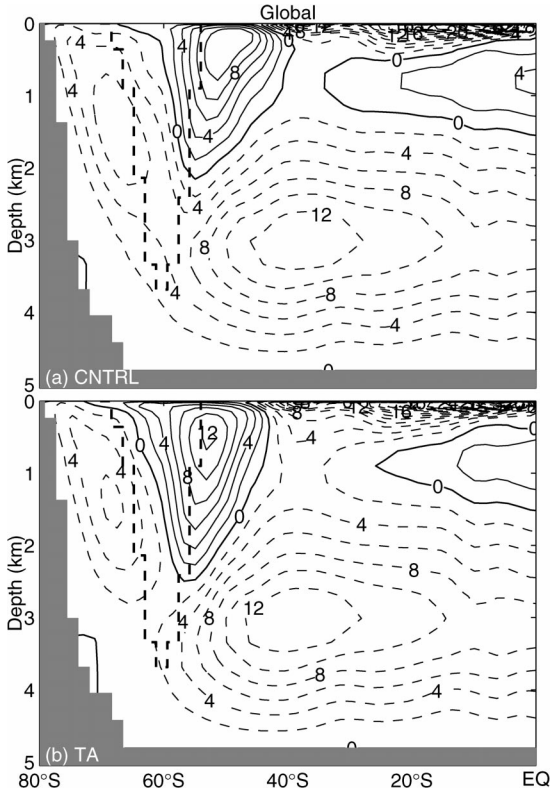

FIG. 3. The MOT in (a) CNTRL and (b) TA, zonally averaged over the entire globe. Contour intervals are 2 Sv; positive is solid, negative is dashed, zero is bold. The bold dashed line denotes the topography across Drake Passage.

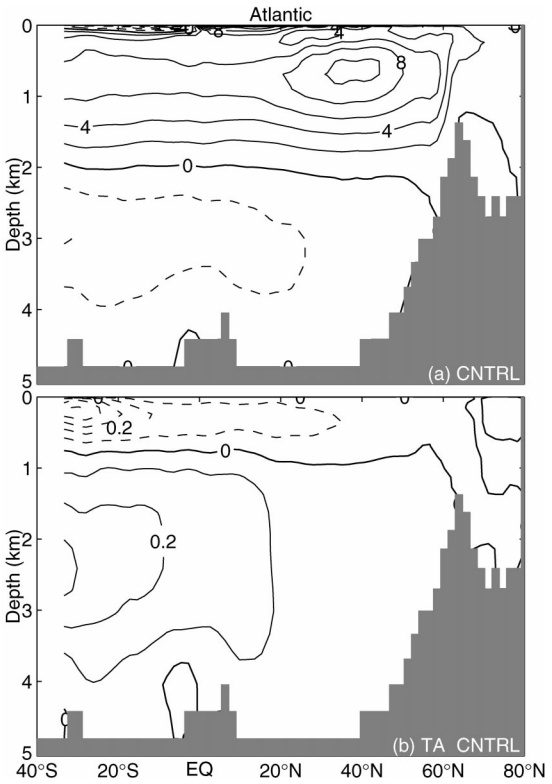

FIG. 4. (a) The MOT in CNTRL (contour interval is 2 Sv) and (b) the difference between CNTRL and TA (contour interval is 0.2 Sv), zonally averaged over the Atlantic basin; positive is solid, negative is dashed, zero is bold.

The meridional overturning (MOT) zonally averaged around the globe and over the Atlantic sector is shown for CNTRL in Figs. 3a and 4a, respectively. Shown here is the MOT combining direct advection and GM advection into a total streamfunction. The model generates MOT in the Deacon cell at a rate of 12.4 Sv and production of AABW and NADW is 7.7 Sv and 10.6 Sv, respectively. Observations suggest that production of AABW is 8.1 Sv (Orsi et al. 1999), in good agreement with the modeled rate. However, observations suggest that the rate of production of NADW is typically 13.3 Sv (Clarke 1984) or greater (e.g., Smethie and Fine 2001), somewhat higher than the modeled overturning. This shortcoming is typical for coarse-resolution ocean models employing the GM scheme (e.g., England and Hirst 1997). Finally, the rate of NADW outflow into the Southern Ocean is 5.8 Sv, located between 1200-m and 2500-m depth at the southern extent of the South Atlantic. Overall, these net transport rates in CNTRL are typical of large-scale ocean and climate models and are in reasonable agreement with observed estimates.

b. Circulation response to the trend anomaly

The horizontal transport streamfunction at the end of TA is shown in Fig. 2b. This field is similar to that at

TABLE 3. Maximum MOT of the Deacon cell and bottom cell, production rates of AABW and NADW, and outflow of NADW in Sv in CNTRL and TA, and the ranges in PA.

MOT feature	Maximum transport (Sv)		Transport range (Sv)
	CNTRL	TA	PA
Deacon cell overturning	11.9	12.4	0.8
Bottom cell overturning	13.6	13.8	6.1
AABW (production)	7.7	6.4	2.2
NADW (production)	10.6	10.6	0.1
NADW (outflow)	6.6	6.7	1.5

the end of CNTRL; however, there are some subtle, but important, changes that are highlighted by the difference field between TA and CNTRL (Fig. 2c). The maximum transports in the Brazil, East Australian, and Agulhas Currents weaken by 4.1, 6.0, and 4.3 Sv, respectively (Table 2). Additionally, there is a band of negative streamfunction anomalies between 40° and 60°S and a positive band south of 60°S. This is because the ACC shifts poleward as the SWWs move to the south. These adjustments are related to the change in wind stress curl as the SWWs move poleward (Fig. 1). In addition, these changes are expected to deepen (shoal) the thermocline and halocline where the wind stress curl anomalies are positive (negative).

The globally averaged MOT is shown for TA in Fig. 3b. The Deacon cell deepens and shifts poleward compared to CNTRL, but the rate of MOT remains virtually unchanged (Table 3). The increased (decreased) wind stress curl north (south) of 60°S results in more downward (upward) local Ekman pumping that has the effect of shifting the Deacon cell poleward, as discussed above. The deepening of the Deacon cell in TA is related to the relative locations of the zonal wind stress maximum and the deepest part of the Drake Passage sill (e.g., England 1992; Toggweiler and Samuels 1995). In particular, as the winds shift poleward in TA, return southward geostrophic flow in the Deacon cell is forced to a greater depth (Fig. 3).

The globally averaged MOT of the AABW cell decreases by 1.1 Sv in TA (Fig. 3b, Table 3). This change is likely to be related to the poleward shift of the upwelling band on the southern side of the Deacon cell. In an idealized modeling study, Rahmstorf and England (1997) found that the rate of production of AABW was sensitive to the strength of the zonal wind stress over the Southern Ocean. Our results suggest that the rate of production of AABW is also sensitive to latitudinal variations of the zonal winds, although the mechanism by which this occurs is unclear.

The difference field of the Atlantic Ocean MOT between CNTRL and that at the end of TA is shown in Fig. 4b. As seen in this diagram, the rate of production of NADW remains virtually unchanged. This is probably because the zonal wind stress at the latitude of Cape Horn (53°S) happens to be largely unchanged at

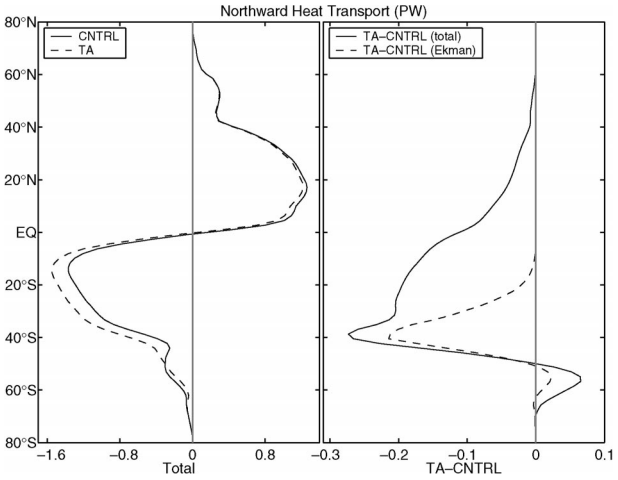

FIG. 5. Northward heat transport (PW) at the end of (left) CNTRL and TA, and (right) the NHT anomaly, TA − CNTRL. The Ekman component of the NHT anomaly is also presented (right).

the end of TA (Fig. 1a). According to the Drake Passage effect (Toggweiler and Samuels 1995) the zonal integral of the zonal wind stress at this latitude controls the rate of production of NADW [when restoring *T* forcing is employed; Rahmstorf and England (1997)].

c. Heat transport response to the trend anomaly

The impact of the trend in the SWWs on the northward heat transport (NHT) is addressed in Fig. 5, showing the zonally averaged NHT at the end of CNTRL and TA along with the difference fields. The most striking change in the NHT is a broad negative anomaly between 50°S and 0°, peaking at −0.27 PW at 40°S. This anomaly represents an increase in southward heat transport or, equivalently, an increase in the northward transport of colder water. This change represents an average increase of 25% between 50°S and the equator. Mechanisms that could explain the negative NHT anomaly within these latitudes include (i) an increased transport in the western boundary currents, (ii) a decreased outflow of NADW, (iii) an increased northward transport of cold water through the wind-driven Ekman layer, and (iv) an increased formation and/or cooling of SAMW/AAIW. As noted each of the Southern Hemisphere subtropical gyres weaken in TA (Fig. 2, Table 2), and the rate of outflow of NADW remains virtually unchanged (Fig. 4, Table 3). These mechanisms can therefore be ruled out. The role of changes in the wind-driven Ekman layer is examined by comparing the Ekman component of the NHT anomaly with the total anomaly in Fig. 5. This shows that changes in Ekman transport contribute significantly to the peak in the anomaly at 40°S with a narrow negative band between 30° and 50°S. However, there is also a broad NHT anomaly that is not directly explained by the Ekman component. Therefore, we suggest that north of 40°S, a substantial fraction of the NHT

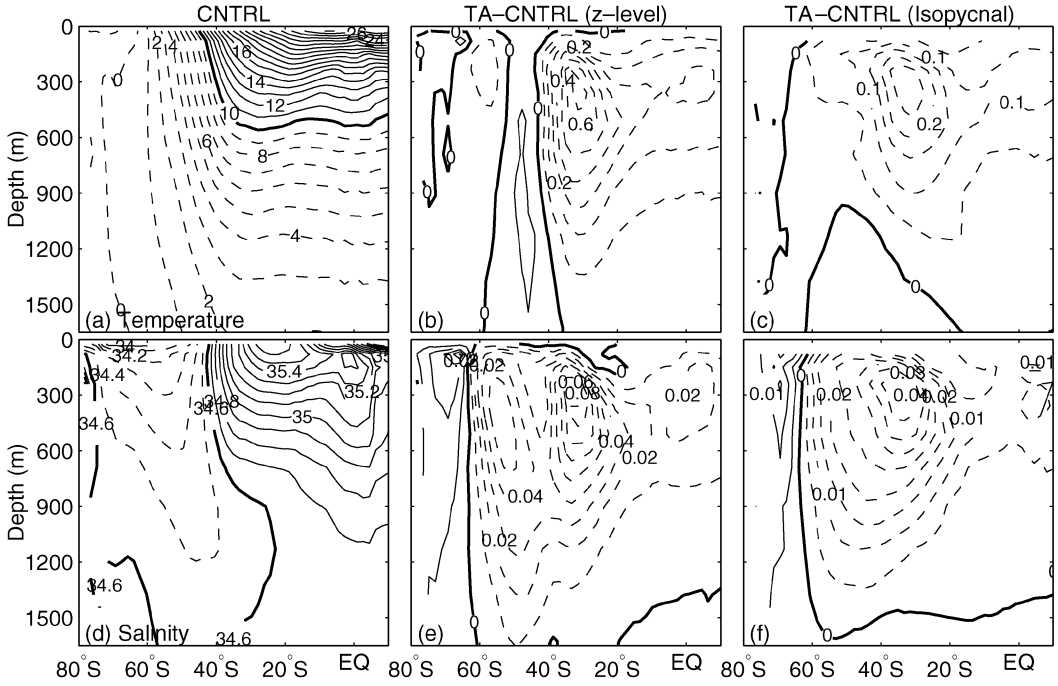

FIG. 6. Zonally averaged fields of (a)–(c) temperature and (d)–(f) salinity showing the final fields at the end of CNTRL in (a) and (d), the difference fields calculated on *z* levels in (b) and (e), and the difference fields calculated on isopycnal surfaces in (c) and (f). For the difference fields, positive is solid, negative is dashed, and zero is bold.

anomaly is likely to be related to changes in water masses. These factors are explored in more detail below.

d. T–S response to the trend anomaly

The zonally averaged *T–S* fields in CNTRL are shown in Figs. 6a,d. The difference fields calculated on both geopotential (*z*-level) and isopycnal coordinates at the end of TA and CNTRL are also shown in Fig. 6. The differences on *z* levels are simply calculated by subtracting the *T–S* fields on the model coordinates (Figs. 6b,e). The differences on isopycnal coordinates are calculated by first interpolating the *T–S* fields to isopycnal surfaces, calculating the differences on those surfaces, and then interpolating back to *z* levels using the isopycnal depths from CNTRL (Figs. 6c,f). These calculations are performed in order to discriminate between changes in the *T–S* properties of water masses and changes due to isopycnal shoaling or deepening, also referred to as ''heaving'' (Bindoff and McDougall 1994). We have done this because we expect there to be some heaving associated with the wind stress curl anomalies in TA. However, we note that most modeling sensitivity studies like ours simply present changes on *z* levels, thereby confounding the physical interpretation.

The zonally averaged fields of tracer MW (sourced at 40°–50°S) and tracer IW (sourced at 50°–60°S) in CNTRL are shown in Fig. 7. The tracer fields in CNTRL show the region of influence of water masses found at the aforementioned latitudes over a 100-yr time scale. We also show the difference fields (TA–CNTRL) on both *z* levels and isopycnal surfaces in Fig. 7. The differences on *z* levels are included here for completeness, however, the differences along isopycnals give a more relevant assessment of the changes in the rate of formation and/or properties of these water masses.

1) AAIW AND DEACON CELL RESPONSE

The tongue of freshwater in Fig. 6d that outcrops at around 60°S denotes the subduction of AAIW. This subduction is primarily represented by tracer IW (Fig. 7d). The *z*-level and isopycnal salinity differences in TA (Figs. 6e,f) demonstrate that there is a freshening coincident with this freshwater tongue from the surface down to 1500 m and between 40° and 65°S. The difference field of tracer IW (Fig. 7f) suggests that there is an increase in the rate of formation of AAIW in TA. In this latitude band the wind stress curl in TA is more positive than in CNTRL. We therefore suggest that the rate of formation increases due to increased downward Ekman pumping via the dynamics described by Stommel (1979). The increased northward transport of colder water in the Ekman layer (Fig. 5) is also likely to enhance convection in the formation regions. The effects of the change in Ekman pumping is evident in the temperature change on *z* levels that shows a narrow band of weak warming between 45° and 50°S. There is also weak cooling on *z* levels south of 50°S, indicating up-

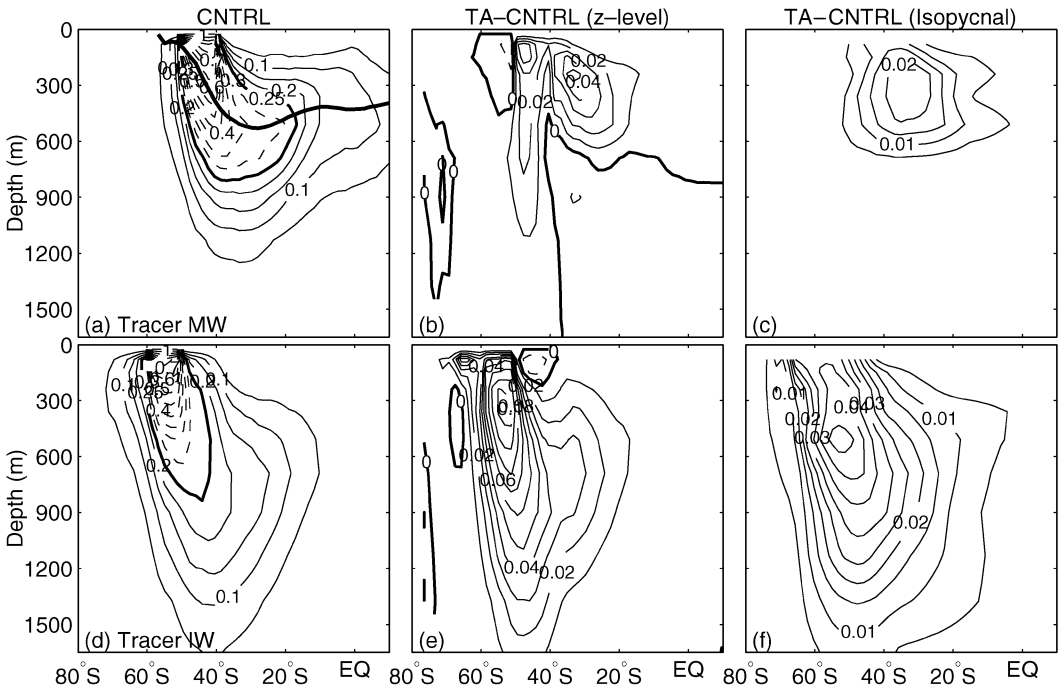

FIG. 7. As in Fig. 6, except for (a)–(c) tracer MW and (d)–(f) tracer IW. Contour intervals are 0.05 in (a) and (d), 0.01 in (b) and (e), and 0.005 in (c) and (f). The zonal mean location of the 26.8-isopycnal, relevant to the analysis in Fig. 8, is shown in (a).

welling of colder water that is related to the negative wind stress curl anomaly at these latitudes. These temperature changes are not evident on isopycnal coordinates, confirming that these anomalies denote heaving (upwelling and downwelling). In fact, our analysis shows that there is a cooling along isopycnal surfaces where there is a warming on *z* levels. This is an example of the counterintuitive situation that Bindoff and McDougall (1994) explain in their paper on diagnosing water-mass change in the ocean.

2) SAMW RESPONSE

Compared to CNTRL, there is a broad region of colder, fresher water north of 40°S in TA with local maxima at 300–500-m depth (Fig. 6). The magnitude of these zonally averaged anomalies on *z* levels peaks at −0.76°C and −0.09 psu at 35°S. On isopycnal surfaces these anomalies peak at −0.28°C and −0.04 psu at 35°S. Notably, the *T*–*S* anomalies are large where the NHT anomalies are large, with similar meridional profiles. Specifically, both peak near 40°S, drop off sharply to the south, gradually decrease to the north, and extend beyond the equator. These oceanic properties are clearly related. The *T*–*S* anomalies lie along the path of SAMW ventilation (Fig. 7a). Because heaving merely represents a depth change of isopycnals, it does not influence the NHT directly. By contrast, changes in the *T*–*S* properties along isopycnal surfaces have the potential to modify the NHT. Comparison of the *T*–*S* anomalies on *z* levels and isopycnal surfaces (Fig. 6) shows that the relative contributions of heaving and *T*–*S* property changes are comparable at midlatitudes. This suggests the importance of changes in SAMW to the increased poleward heat transport in TA (Fig. 5).

The zonally averaged field of tracer MW at the end of CNTRL (Fig. 7a) shows the subduction of SAMW to depths of 300–600 m and subsequent northward transport. This field covers the same region as the negative *T*–*S* anomalies north of 40°S (Fig. 6), again affirming the importance of changes of SAMW there. The difference fields of tracer MW (Fig. 7c) are small, implying that the formation rate of SAMW does not change significantly. We therefore conclude that the cooling of SAMW (Fig. 6c), rather than changes in its rate of formation, is primarily responsible for the negative NHT anomaly in TA. Moreover, the Ekman component of the NHT anomaly (Fig. 5) indicates that there is an increase in the northward advection of cold water in the Ekman layer around 40°S. This is directly related to the imposed wind stress anomaly in TA. The increased transport of cold water towards the latitude band where SAMW forms explains the changes in *T*–*S* properties near the surface that subsequently modify SAMW at depth. The influence of Ekman transport on SAMW formation has recently been documented by Rintoul and England (2002).

To establish where the cooling and freshening of SAMW occurs, we examine the *T*–*S* changes along the 26.8-isopycnal surface (Figs. 8a,b) that nominally de-

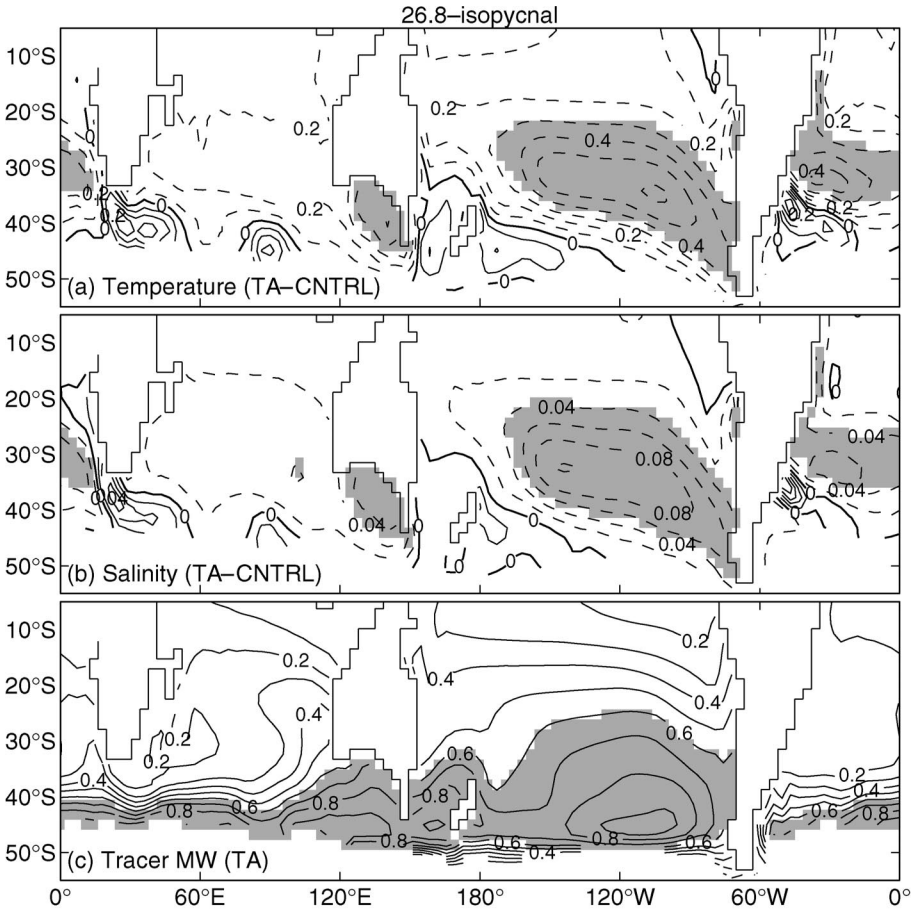

FIG. 8. (a) Temperature and (b) salinity differences (TA − CNTRL) at the end of each experiment and (c) the final field of tracer MW (nominally representing SAMW) at the end of TA, along the 26.8-isopycnal surface. Contour intervals are 0.1°C, 0.02 psu, and 0.1. Regions where $\Delta T < -0.3$°C, $\Delta S < -0.04$ psu, and tracer MW exceeds 0.5 are highlighted in gray.

notes SAMW (McCartney 1977). The location of the zonally averaged 26.8-isopycnal is shown in Fig. 7a. In our model, the 26.8-isopycnal outcrops between 40° and 50°S, except off South America where it outcrops slightly farther south. This analysis shows that the cooling (up to −0.6°C) and freshening (up to 0.1 psu) of SAMW is most evident in the central-south Pacific. These anomalies appear to originate in the southeast Pacific, off the coast of Chile. This region has previously been identified as a site of SAMW formation (McCartney 1977; England et al. 1993). The tracer MW field along the 26.8-isopycnal (Fig. 8c) confirms that SAMW is most abundant in the South Pacific, coincident with the large *T*–*S* changes there.

3) AABW RESPONSE

South of 55°S there is a positive NHT anomaly in TA (Fig. 5). Part of this is related to changes in Ekman transport; however, most of it can be explained by a 20% decrease in production of AABW in TA (6.4 Sv) compared to CNTRL (7.7 Sv). A reduction in MOT of AABW means weaker upper-ocean advection towards Antarctica and a decrease in the northward transport of cold water at depth. This yields a positive NHT anomaly. Clearly, the changes in the winds in TA have a significant impact on the rate of production of AABW. Interestingly, in an observational study of chlorofluorocarbon inventories, Broecker et al. (1999) concluded that the rate of AABW production has decreased significantly over the past century. It could be that a small part of this reduction is related to the concurrent long-term changes in the latitude band of the SWWs.

e. Periodic anomaly experiment

The range of the horizontal transport streamfunction in PA (Fig. 9) shows that most of the variability generated by the periodic latitudinal shift in the zonal winds occurs in the ACC region (40°–60°S). There are local maxima near the Kerguelen Plateau (90°E), the Campbell Plateau (170°W), and the Brazil–Malvinas conflu-

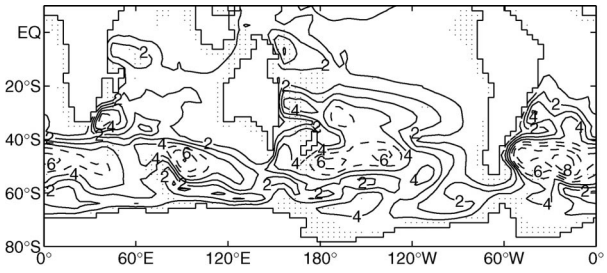

FIG. 9. Horizontal transport streamfunction range for PA. The contour interval is 1 Sv; contours of less (greater) than 4.5 Sv are solid (dashed). Stippled areas denote regions shallower than 3000 m.

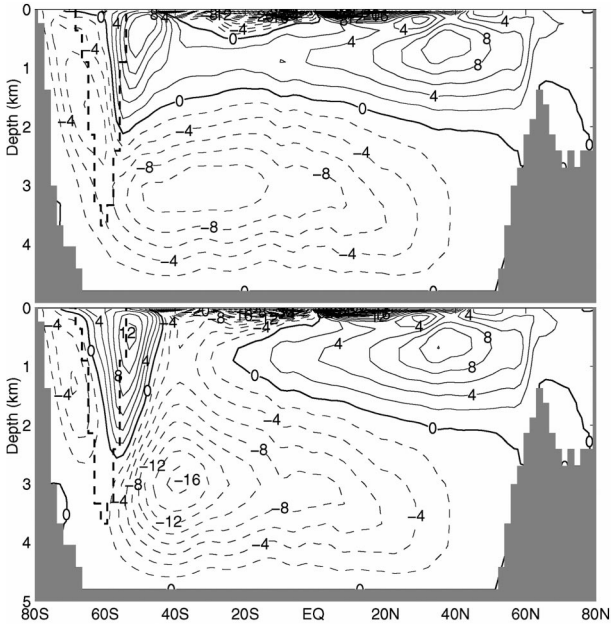

FIG. 10. Globally averaged MOT during the (top) northernmost and (bottom) southernmost excursions of the SWWs in PA. Contour interval is 2 Sv; positive is solid, negative is dashed, zero is bold. The bold dashed line denotes the topography across the Drake Passage.

ence (50°W), where the ACC path is known to be influenced by geographic and topographic features (Chelton et al. 1990; England and Garcon 1994). Additionally, PA shows considerable variability in the East Australian, Brazil, and Agulhas Current regions (see also Table 2). This variability is consistent with the changes in the wind stress curl (Fig. 1b), as explained for TA above.

The global MOT streamfunction during the northernmost and southernmost excursions of the zonal wind belt in PA is shown in Fig. 10. During the northernmost excursion the winds are identical to CNTRL, so at that point the MOT is similar to CNTRL. Any differences are due to transient adjustments to the fluctuating winds. Similarly, the MOT during the southernmost excursion is similar to that at the end of TA. However, one significant difference is the maximum rate of overturning of the bottom cell, where the MOT increases by 6.1 Sv during PA (Fig. 10 and Table 3). This change must indicate a transient adjustment of the deep ocean overturning to shifting winds because in TA, where the winds change more slowly, the bottom cell is mostly unchanged from CNTRL.

The quantitative MOT response in PA is summarized in Fig. 11. This figure shows the latitude of the maximum westerly wind stress varying by 5.4° with a period of 11 yr. The maximum MOT of the AABW cell is clearly periodic with a range of 2.2 Sv (Fig. 11b, Table 3). There is virtually no phase lag between the imposed wind fluctuations and the AABW production that decreases (increases) during poleward (equatorward) excursions of the wind field. This result is consistent with TA. The rapid AABW response to wind forcing indicates that the oscillating AABW rate must not be controlled by interior mixing, but by shifts in the location of the wind-driven overturning axes.

The variations of NADW production in PA are negligible, owing to the near-constant zonal wind stress field at the latitude of Cape Horn (Toggweiler and Samuels 1993, 1995). In contrast, the variations of NADW outflow in the South Atlantic are periodic with a range of 1.5 Sv (Fig. 11c, Table 3). According to the theory developed by Nof (2000), the outflow rate is controlled by the South Atlantic zonal wind stress at the latitude of the southern tip of Africa (35°S). The periodic trend of the NADW outflow in PA is consistent with Nof's theory. The variations of the Deacon cell MOT in PA are also periodic; however, the range of 0.8 Sv is small compared to the total MOT (Fig. 11d, Table 3).

The NHT anomalies in PA show that, when the winds shift poleward, the NHT decreases by 0.3–0.4 PW (Fig. 12). This response is consistent with the results from TA, where the poleward shift of the Deacon cell transports colder water equatorward, resulting in colder SAMW that gets subducted at midlatitudes. Interestingly, there is also a long-term trend in PA. At the start of PA, the maximum magnitude of the negative NHT anomaly is 0.3 PW; by the end of PA, the maximum magnitude is in excess of 0.4 PW. This is because PA only involves southward shifts in the wind axis relative to CNTRL. Therefore the time-averaged zonal wind stress in PA is not equivalent to that in CNTRL. In addition to the periodic changes, there is also a long-term poleward shift in PA (half that simulated in TA). Our findings that the NHT is sensitive to the latitude of the SWWs are qualitatively consistent with those of Hall and Visbeck (2002), with both studies showing a change in the sign of the anomaly at midlatitudes.

4. Discussion

The model experiments presented above are not hindcasts of the ocean's circulation. However, in order to assess the possibility that changes in the latitude of the

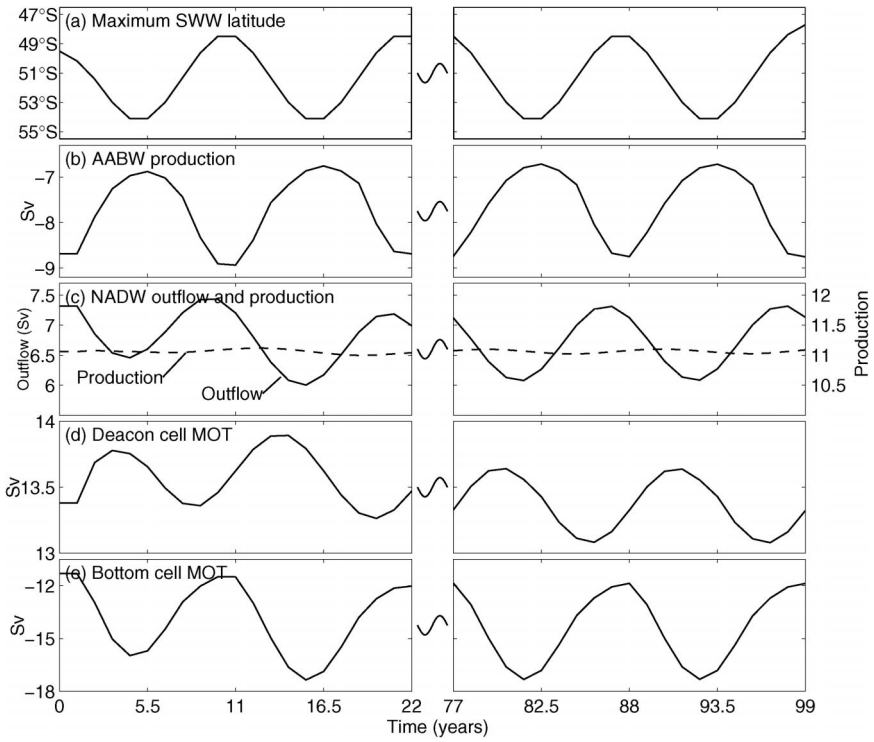

FIG. 11. Time series for the (left) first two and (right) last two 11-yr cycles in PA, showing (a) the latitude of the maximum zonal wind stress, (b) the maximum rate of production of AABW, (c) the maximum outflow (solid) and rate of production (dashed) of NADW, and the maximum rate of MOT in (d) the Deacon cell and (e) the bottom cell.

SWWs may help explain some part of the observed midlatitude cooling trends at intermediate water depths reported by Gille (2002) and T03, we present a comparison between the observed trends over the last 50 yr and modeled trends in the TA experiment (Fig. 13). Additionally, we present the modeled temperature range at 900-m depth in PA (Fig. 14) in order to assess whether periodic variations in the SWWs could provide a fea-

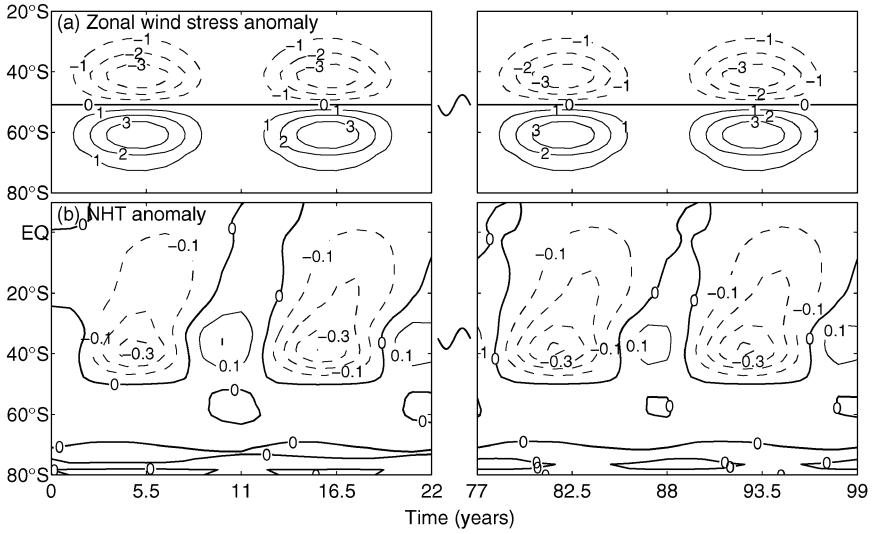

FIG. 12. Time–latitude contour plots of (a) the zonally averaged zonal wind stress anomaly (Pa × 100) and (b) the northward heat transport anomaly (PW) for the first two and last two 11-yr cycles in PA. Contour intervals are 1 Pa × 100 and 0.1 PW; positive is solid, negative is dashed, zero is bold.

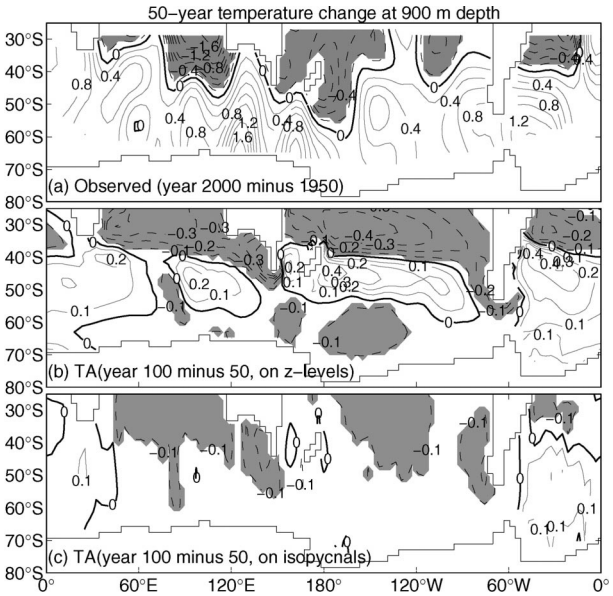

FIG. 13. (a) Observed temperature change at 900-m depth between 1950 and 2000 (after Gille 2002); and the modeled temperature change on (b) *z* levels and (c) isopycnals between year 50 and 100 in TA. Contour intervals are 0.2°C in (a) and 0.1°C in (b) and (c); dashed is negative (cooling), solid is positive (warming), and bold is zero; regions of less than −0.1°C are highlighted in gray. The strongest modeled cooling occurs near Tasmania with a magnitude of 0.62° and 0.28°C on *z* levels and isopycnal surfaces, respectively.

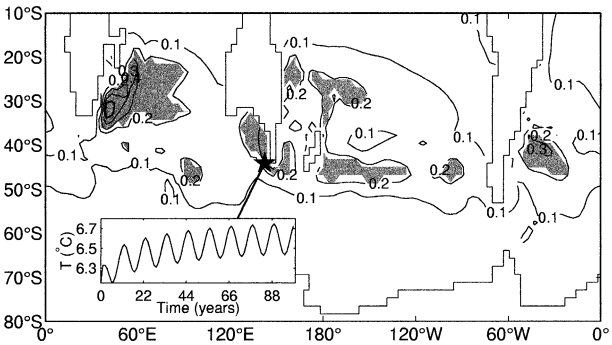

FIG. 14. Temperature range at 900-m depth in PA analyzed on *z* levels. Contour interval is 0.1°C; regions with a range of greater than 0.2°C are highlighted in gray. The maximum temperature range off western Tasmania is 0.4°C. The inset shows the time series of temperature at 900-m depth in the vicinity of the measurements reported by T03.

sible explanation for the observed periodic temperature fluctuations reported by Thresher et al.

This study was motivated in part by recent observations of long-term temperature trends at intermediate water depths (centered around 900-m) in the Southern Ocean (Gille 2002; T03). The observations suggest that there has been a significant intermediate depth cooling at midlatitudes over the past 50–100 years. In addition, Gille noted larger than expected warming at high latitudes. The yearly temperature trends over the last 50 yr calculated by Gille are objectively analyzed onto the model grid using an *e*-folding scale of 5.4° latitude and 10.8° longitude (i.e., three grid cells in each direction). These length scales are chosen in order to filter out scales that are unresolved by the model. The objectively analyzed observed trends are subsequently scaled to a 50-yr temperature anomaly (Fig. 13a). Notably, Gille's observations were recorded along pressure levels. Therefore, they contain variations related to heaving as well as changes in water mass properties (Bindoff and McDougall 1994). For comparison, the modeled temperature change calculated on both *z* levels and isopycnal surfaces (centered at 900-m depth) for the last 50 yr of TA is presented in Figs. 13b,c. In these plots, the regions where there is more than 0.1°C of cooling are highlighted. The observed cooling trend north of 40°S mostly coincides with regions of cooling in TA. However, the magnitude of cooling found in the model is a little weaker than observed. When the effects of heaving are removed, the model shows cooling of only about 0.1°C at midlatitudes, with the strongest cooling of 0.28°C off Tasmania. Thus, at this depth, temperature changes in TA are mostly a result of heaving of isopycnals. Heave effects may also significantly contribute to the temperature trends observed by Gille (2002). Either way, a substantial fraction of the cooling trend detected by Gille north of 40°S might be explained by a southward shift in the zonal wind stress field over the past half-century.

Between 40° and 60°S, TA shows warming on *z* levels at magnitudes near that observed (Fig. 13). In contrast to the cooling north of 40°S, almost all of the warming vanishes when the effects of heaving are eliminated. This leads one to speculate about how much of the warming observed at 40°–60°S by Gille (2002) represents changes in water mass properties forced by anthropogenic climate change and how much is simply related to heaving of isotherms due to changes in the wind field. In contrast, the warming observed south of 60°S (Fig. 13a) is unlikely to be caused by latitudinal shifts in the SWWs, with the TA experiment showing mostly weak cooling there (Fig. 13b).

To explain the cooling at midlatitudes, Gille (2002) suggested that the decreased wind stress curl that is evident in the National Centers for Environmental Prediction–National Center for Atmospheric Research (NCEP–NCAR) reanalysis south of 30°S (Kalnay et al. 1996) may lead to reduced downwelling of warmer water into the interior. In our trend anomaly experiment, the poleward shift of the SWWs corresponds to a reduced wind stress curl between 30° and 40°S. However, we find that the cooling in the model at 900-m depth results from a change in AAIW (Fig. 7f) that is related to changes in the Ekman transport and pumping (or heave) near the formation regions.

T03 analyzed variations in the elemental and isotopic compositions of deep water octocorals to infer a temperature decrease of 1.4°–1.9°C at around 1000-m depth

near Tasmania over the past 100 years or so. They hypothesized that this might be due to a poleward shift of the SWWs over the last century. In our model we find that a 5.4° poleward shift in the SWWs drives a 1.1°C cooling at 900-m depth near Tasmania. This suggests that part of the observed cooling may be related to a poleward shift of the SWWs that has the effect of shifting the Ekman-driven flow poleward, resulting in increased formation and cooling of AAIW.

In addition to the observed cooling trend, T03 note temperature fluctuations with a range of 0.6°C and a quasi-decadal, or longer, cycle that appears to be in phase with solar events. They hypothesize that solar events may modulate the SWWs, through differential heating of the stratosphere, which in turn modifies the ocean's temperature at intermediate water depths. We note that controversy remains on sunspot-related issues (e.g., Meadows 1975; Burroughs 1992); however, we refer to the PA experiment as an initial assessment of the feasibility of the Thresher et al. hypothesis. More generally, we regard PA as an examination of the impact of natural, quasi-decadal variations in the SWWs on intermediate-water mass properties. The temperature range at 900-m depth in PA is shown in Fig. 14. The modeled temperature fluctuations have a range of 0.4°C off Tasmania in the vicinity of the measurements referred to above. Considering the differences in scales resolved by the point source measurements and our coarse-resolution simulation, the model fluctuations compare favorably with the observed range of 0.6°C. Again, this suggests that variations in the SWWs may have contributed to the observed intermediate temperature changes via Ekman flow and subduction.

The map of temperature ranges in PA (Fig. 14) shows that large variations at 900-m depth appear over a substantial fraction of the South Pacific and South Atlantic basins, particularly between 40° and 50°S. However, in the model region where the temperature proxy was measured (off Tasmania) there is unusual sensitivity to the imposed periodic wind shift. Other regions of high sensitivity include the Agulhas and Brazil–Malvinas confluence regions, where we expect heaving is important.

5. Conclusions

The goal of our study was to assess ocean sensitivity to subtle changes in the latitude of the SWW field. Such an analysis has never been undertaken before. In addition, our experiments were motivated by recent observations of long-term cooling and quasi-decadal fluctuations of temperature at intermediate depths at midlatitudes in the Southern Ocean (Gille 2002; T03). To examine the hypothesis that these changes are caused by a variation in the latitude of the SWWs, we utilize a coarse-resolution World Ocean model where the winds either trend poleward by 5.4° over 100-yr or shift periodically by 5.4° with an 11-yr cycle. In the trend experiment we find that the poleward heat transport in the Southern Hemisphere increases by an average of 25% between 50°S and the equator. As expected, the northward Ekman drift in the Deacon cell shifts poleward beneath the SWWs, resulting in colder water being transported northward toward the regions where SAMW and AAIW are formed. These factors cause SAMW to cool by up to 0.5°C and freshen by 0.08 psu in the central-south Pacific. We also find a change in the rate of formation of AAIW that results in cooling of up to 0.5°C on z levels at midlatitude intermediate depths. Of this cooling, around 0.1°C is due to changes in T–S properties along isopycnals, with the strongest cooling occurring off Tasmania, where it peaks at 0.28°C. The model z-level temperature changes are comparable to the cooling at midlatitudes reported by Gille (2002) and T03. We therefore suggest that a poleward shift of the SWWs, like that observed over the last century (Das 1956; Thresher 2002), is a feasible explanation for the observed cooling at intermediate depths.

In an experiment where the SWWs shift periodically over 5.4° latitude, the modeled ocean responds rapidly, with -0.3 to -0.4 PW anomalies in the NHT, 2 Sv changes in AABW production, and 1.5 Sv changes in NADW outflow. The response of temperature at intermediate depths is nonuniform, with localized fluctuations of up to 0.4°C near Tasmania and in the Agulhas and Malvinas–Brazil Currents. These localized model fluctuations are similar to those reported by T03 near Tasmania. However, we find the response at their observation site to be quite high compared to other regions of the Southern Ocean. As such, the aforementioned observations may have measured a location of unusually large ocean response, rather than one that is representative of other longitudes. Despite this, we find that periodic shifts in the latitude of the SWWs are a feasible explanation for part of their observations.

One important finding of our study is that natural (PA) variations in the SWWs have the capacity to alter interior ocean T–S properties significantly. This has implications for detection and attribution of climate change, as SAMW and AAIW have been suggested as water masses sensitive to CO_2 forcing (Banks and Wood 2002). In our model experiments, we have shown that latitudinal changes in the SWWs can generate temperature fluctuations of the order of 0.4°C decade^{-1} at 900-m depth. While we acknowledge that the latitudinal range of 5.4° for the decadal wind variations in PA is somewhat arbitrary, we note that several observational studies have reported temperature changes of similar magnitudes and implied that their findings were evidence of global warming (e.g., Bindoff and Church 1992; Wong et al. 1999; Levitus et al. 2000; Gille 2002). We have demonstrated that a substantial fraction of such changes might be related to natural variability of the climate system.

Acknowledgments. This research was supported by the Australian Research Council. Steve Rintoul and

John Fyfe are acknowledged for helpful discussions; and Ron Thresher and coauthors are thanked for making their observations known to us prior to publication of their manuscript. Sarah Gille is acknowledged for providing the processed fields of observed temperature trends used to construct Fig. 13a; and two anonymous reviewers are acknowledged for constructive criticism of this manuscript. Model calculations were carried out on the Australian Partnership for Advanced Computing (APAC) National Facility.

REFERENCES

Banks, H., and R. Wood, 2002: Where to look for anthropogenic change in the ocean. *J. Climate,* **15,** 879–891.

Beal, L. M., and H. L. Bryden, 1999: The velocity and vorticity structure of the Agulhas Current at 32°S. *J. Geophys. Res.,* **104,** 5151–5176.

Bindoff, N. L., and J. A. Church, 1992: Warming of the water column in the southwest Pacific Ocean. *Nature,* **357,** 59–62.

——, and T. J. McDougall, 1994: Diagnosing climate change and ocean ventilation using hydrographic data. *J. Phys. Oceanogr.,* **24,** 1137–1152.

Broecker, W. S., S. Sutherland, and T.-H. Peng, 1999: A possible 20th-century slowdown of Southern Ocean deep water formation. *Science,* **286,** 1132–1135.

Bryan, K., 1969: A numerical method for the study of the circulation of the World Ocean. *J. Comput. Phys.,* **3,** 347–376.

——, and L. J. Lewis, 1979: A water mass model of the World Ocean. *J. Geophys. Res.,* **84,** 2503–2517.

Burroughs, W. J., 1992: *Weather Cycles: Real or Imaginary?* Cambridge University Press, Cambridge, 99 pp.

Cai, W., P. H. Whetton, and D. J. Karoly, 2003: The response of the Antarctic Oscillation to increasing and stabilized atmospheric CO_2. *J. Climate,* **16,** 1525–1538.

Carleton, A. M., 2003: Atmospheric teleconnections involving the Southern Ocean. *J. Geophys. Res.,* **108**, 8080, doi:10.1029/2000JC000379.

Chelton, D. B., M. G. Schlax, D. L. Witter, and J. G. Richman, 1990: Geostat altimeter observations of sea surface circulation of the southern ocean. *J. Geophys. Res.,* **95,** 17 877–17 903.

Clarke, R. A., 1984: Transport through the Cape Farewell–Flemish Cap section. *Rapp. V. P. Reun. Cons. Int. Explor.,* **185,** 120–130.

Cox, M. D., 1984: A primitive equation, three-dimensional model of the ocean. GFDL Ocean Group Tech. Rep. 1, 143 pp.

Danabasoglu, G., and J. C. McWilliams, 1995: Sensitivity of the global ocean circulation to parameterizations of mesoscale tracer transports. *J. Climate,* **8,** 2967–2987.

———, ———, and P. R. Gent, 1994: The role of mesoscale tracer transports in the global ocean circulation. *Science,* **264,** 1123–1126.

Das, S. C., 1956: Statistical analysis of Australian pressure data. *Aust. J. Phys,* **9,** 394–399.

England, M. H., 1992: On the formation of Antarctic Intermediate and Bottom Water in ocean general circulation models. *J. Phys. Oceanogr.,* **22,** 918–926.

——, 1993: Representing the global-scale water masses in ocean general circulation models. *J. Phys. Oceanogr.,* **23,** 1523–1552.

——, 1995: The age of water and ventilation timescales in a global ocean model. *J. Phys. Oceanogr.,* **25,** 2756–2777.

——, and V. C. Garcon, 1994: South Atlantic circulation in a world ocean model. *Ann. Geophys.,* **12,** 812–825.

——, and A. C. Hirst, 1997: Chlorofluorocarbon uptake in a World Ocean model, 2. Sensitivity to surface thermohaline forcing and subsurface mixing parameterization. *J. Geophys. Res.,* **102,** 15 709–15 731.

——, J. S. Godfrey, A. C. Hirst, and M. Tomczak, 1993: The mechanism for Antarctic Intermediate Water renewal in a World Ocean model. *J. Phys. Oceanogr.,* **23,** 1553–1560.

Fieux, M., R. Molcard, and A. G. Ilahude, 1996: Geostrophic transport of the Pacific–Indian Oceans throughflow. *J. Geophys. Res.,* **101,** 12 421–12 432.

Fyfe, J. C., 2003: Separating extratropical zonal wind variability and mean change. *J. Climate,* **16,** 863–874.

Fyfe, J. C., G. J. Boer, and G. M. Flato, 1999: The Arctic and Antarctic Oscillations and their projected changes under global warming. *Geophys. Res. Lett.,* **26,** 1601–1604.

Gent, P. R., and J. C. McWilliams, 1990: Isopycnal mixing in ocean circulation models. *J. Phys. Oceanogr.,* **20,** 150–155.

——, J. Willebrand, T. J. McDougall, and J. C. McWilliams, 1995: Parameterizing eddy-induced tracer transports in ocean circulation models. *J. Phys. Oceanogr.,* **25,** 463–474.

Gille, S. T., 2002: Warming of the Southern Ocean since the 1950s. *Science,* **295,** 1275–1277.

Gnanadesikan, A., and R. W. Hallberg, 2000: On the relationship of the Circumpolar Current to Southern Hemisphere winds in coarse-resolution ocean models. *J. Phys. Oceanogr.,* **30,** 2013–2034.

Hall, A., and M. Visbeck, 2002: Synchronous variability in the Southern Hemisphere atmosphere, sea ice, and ocean resulting from the Annular Mode. *J. Climate,* **15,** 3043–3057.

Harris, G. P., P. Davies, M. Nunez, and G. Meyers, 1988: Interannual variability in climate and fisheries in Tasmania, Australia. *Nature,* **333,** 754–757.

Hartmann, D. L., and F. Lo, 1998: Wave-driven zonal flow vacillation in the Southern Hemisphere. *J. Atmos. Sci.,* **55,** 1303–1315.

——, J. M. Wallace, V. Limpasuvan, D. W. J. Thompson, and J. R. Holton, 2000: Can ozone depletion and greenhouse warming interact to produce rapid climate change? *Proc. Natl. Acad. Sci. USA,* **97,** 1412–1417.

Hellerman, S., and M. Rosenstein, 1983: Normal monthly wind stress over the world ocean with error estimates. *J. Phys. Oceanogr.,* **13,** 1093–1104.

Hirst, A. C., and T. J. McDougall, 1996: Deep water properties and surface flux as simulated by a Cartesian model including eddy-induced advection. *J. Phys. Oceanogr.,* **26,** 1320–1343.

Jones, J. M., and M. Widmann, 2003: Instrument- and tree-ring-based estimates of the Antarctic Oscillation. *J. Climate,* **16,** 3511–3524.

Kalnay, E., and Coauthors, 1996: The NCEP/NCAR 40-Year Reanalysis Project. *Bull. Amer. Meteor. Soc.,* **77,** 437–471.

Kushner, P. J., I. M. Held, and T. L. Delworth, 2001: Southern Hemisphere atmospheric circulation response to global warming. *J. Climate,* **14,** 2238–2249.

Levitus, S., 1982: *Climatological Atlas of the World.* NOAA Prof. Paper 13, 173 pp. and 17microfiche.

——, J. I. Antonov, T. P. Boyer, and C. Stephens, 2000: Warming of the world oceans. *Science,* **287,** 2225–2229.

Limpasuvan, V., and D. L. Hartmann, 1999: Eddies and the annular modes of climate variability. *Geophys. Res. Lett.,* **26,** 3133–3136.

Maamaatuaiahutapu, K., V. Garcon, C. Provost, and H. Mercier, 1998: Transports of the Brazil and Malvinas Currents at their confluence. *J. Mar. Res.,* **56,** 417–438.

Mata, M. M., M. Tomczak, S. Wijffels, and J. Church, 2000: East Australian current volume transports at 30°S: Estimates from the WOCE hydrographic section PR11/P6 and PCM3 current meter array. *J. Geophys. Res.,* **105,** 28 509–28 526.

McCartney, M. S., 1977: Subantarctic Mode Water. *A Voyage of Discovery, George Deacon 70th Anniversary Volume,* M. Angel, Ed., Pergamon Press, 103–119.

McDermott, D., 1996: The regulation of Northern Hemisphere overturning by Southern Hemisphere winds. *J. Phys. Oceanogr.,* **26,** 1234–1255.

McDougall, T. J., and J. A. Church, 1986: Pitfalls with the numerical representation of isopycnal and diapycnal mixing. *J. Phys. Oceanogr.,* **16,** 196–199.

Meadows, A. J., 1975: A hundred years of controversy over sunspots and weather. *Nature,* **256,** 95–97.

Nof, D., 2000: Does the wind control the import and export of the South Atlantic? *J. Phys. Oceanogr.,* **30,** 2650–2667.

Orsi, A. H., T. Whitworth III, and W. D. Nowlin Jr., 1995: On the meridional extent and fronts of the Antarctic Circumpolar Current. *Deep-Sea Res.,* **42,** 641–673.

——, G. C. Johnson, and J. L. Bullister, 1999: Circulation, mixing and production of Antarctic Bottom Water. *Progress in Oceanography,* Vol. 43, Pergamon, 55–109.

Pacanowski, R. C., 1995: MOM2 documentation user's guide and reference manual. GFDL Ocean Group Tech. Rep. 3, 232 pp.

Rahmstorf, S., and M. H. England, 1997: Influence of Southern Hemisphere winds on North Atlantic Deep Water flow. *J. Phys. Oceanogr.,* **27,** 2040–2054.

Redi, M. H., 1982: Oceanic isopycnal mixing by coordinate rotation. *J. Phys. Oceanogr.,* **12,** 1154–1158.

Ribbe, J., 1999: On wind-driven mid-latitude convection in ocean general circulation models. *Tellus,* **51A,** 517–525.

Rintoul, S. R., and M. H. England, 2002: Ekman transport dominates local air–sea fluxes in driving variability of subantarctic mode water. *J. Phys. Oceanogr.,* **32,** 1308–1321.

Robitaille, D. Y., and A. J. Weaver, 1995: Validation of sub-grid scale mixing schemes using CFCs in a global ocean model. *Geophys. Res. Lett.,* **22,** 2917–2920.

Rogers, J. R., and H. van Loon, 1982: Spatial variability of SLP and 500 mb height anomalies over the Southern Hemisphere. *Mon. Wea. Rev.,* **110,** 1375–1392.

Smethie, W. M., and R. A. Fine, 2001: Rates of North Atlantic Deep Water formation from chlorofluorocarbon inventories. *Deep-Sea Res.,* **48,** 189–215.

Smith, S. R., and C. R. Stearns, 1993: Antarctic climate anomalies surrounding the minimum in the Southern Oscillation Index. *Antarctic Meteorology and Climatology: Studies Based on Automatic Weather Stations,* D. H. Bromwich and C. R. Stearns, Eds., Antarctic Research Series, Vol. 61, Amer. Geophys. Union, 149–174.

Smith, W. H. F., and D. T. Sandwell, 1997: Global seafloor topography from satellite altimetry and ship depth soundings. *Science,* **277,** 1957–1962.

Stommel, H., 1957: A survey of ocean current theory. *Deep-Sea Res.,* **4,** 149–184.

——, 1979: Determination of water-mass properties of water pumped down from the Ekman layers to the geostrophic flow below. *Proc. Natl. Acad. Sci. USA,* **76,** 3051–3055.

Thompson, D. W. J., and S. Solomon, 2002: Interpretation of recent Southern Hemisphere climate change. *Science,* **296,** 895–899.

——, J. M. Wallace, and G. C. Hegerl, 2000: Annular modes in the extratropical circulation. Part II: Trends. *J. Climate,* **13,** 1018–1036.

Thresher, R. E., 2002: Solar correlates of Southern Hemisphere mid-latitude climate variability. *Int. J. Climate,* **22,** 901–915.

Toggweiler, J. R., and B. Samuels, 1993: Is the magnitude of the deep outflow from the Atlantic Ocean actually governed by Southern Hemisphere winds? *The Global Carbon Cycle,* M. Heimann, Ed., Springer, 303–331.

——, and ——, 1995: Effect of Drake Passage on the global thermohaline circulation. *Deep-Sea Res.,* **42,** 477–500.

van Loon, H., and K. Labitzke, 1998: The global range of the stratospheric decadal wave. Part I: Its association with the sunspot cycle in summer and in the annual mean, and with the troposphere. *J. Climate,* **11,** 1529–1537.

Watterson, I. G., 2000: Southern midlatitude zonal wind vacillation and its interaction with the ocean in GCM simulations. *J. Climate,* **13,** 562–578.

Whetton, P., M. H. England, S. P. O'Farell, I. G. Watterson, and A. B. Pittock, 1996: Global comparison of the regional rainfall results of enhanced greenhouse coupled and mixed layer ocean experiments: Implications for climate change scenario development. *Climatic Change,* **33,** 497–519.

White, W. B., and R. G. Peterson, 1996: An Antarctic circumpolar wave in surface pressure, temperature and sea-ice extent. *Nature,* **380,** 699–702.

Whitworth, T., III, 1983: Monitoring the transport of the Antarctic Circumpolar Current at the Drake Passage. *J. Phys. Oceanogr.,* **13,** 2045–2057.

——, W. D. Nowlin, and S. J. Worley, 1982: The net transport of the Antarctic Circumpolar Current through the Drake Passage. *J. Phys. Oceanogr.,* **12,** 960–971.

Wong, A. P. S., N. L. Bindoff, and J. A. Church, 1999: Large-scale freshening of intermediate waters in the Pacific and Indian Oceans. *Nature,* **400,** 440–443.